

# Super-rough glassy phase of the random field XY model in two dimensions

A. Perret<sup>1</sup>, Z. Ristivojevic<sup>2</sup>, P. Le Doussal<sup>2</sup>, G. Schehr<sup>1</sup>, and K. J. Wiese<sup>2</sup>

<sup>1</sup>Laboratoire de Physique Théorique et Modèles Statistiques,  
CNRS-Université Paris-Sud, Bât. 100, 91405 Orsay France and

<sup>2</sup>Laboratoire de Physique Théorique-CNRS, Ecole Normale Supérieure, 24 rue Lhomond, 75005 Paris, France

We study both analytically, using the Renormalization Group (RG) to two loop order, and numerically, using an exact polynomial algorithm, the disorder-induced glass phase of the two-dimensional XY model with quenched random symmetry-breaking fields and without vortices. In the super-rough glassy phase, i.e. below the critical temperature  $T_c$ , the disorder and thermally averaged correlation function  $B(r)$  of the phase field  $\theta(\mathbf{x})$ ,  $B(r) = \overline{[\theta(\mathbf{x}) - \theta(\mathbf{x} + \mathbf{r})]^2}$  behaves, for  $r \gg a$ , as  $B(r) \simeq A(\tau) \log^2(r/a)$  where  $r = |\mathbf{r}|$  and  $a$  is a microscopic length scale. We derive the RG equations up to cubic order in  $\tau = (T_c - T)/T_c$  and predict the universal amplitude  $A(\tau) = 2\tau^2 - 2\tau^3 + \mathcal{O}(\tau^4)$ . Using an exact polynomial algorithm on an equivalent dimer version of the model we compute  $A(\tau)$  numerically and obtain a remarkable agreement with our analytical prediction, up to  $\tau \approx 0.5$ .

Disordered elastic systems are relevant to describe various experimental situations ranging, for interfaces, from domain walls in ferromagnetic [1] or ferroelectric [2] systems, contact lines in wetting [3] to propagating cracks [4] and, for periodic structures, from vortex lattices in type-II superconductors [5] and Wigner crystals [6], to electronic crystals displaying charge or spin density waves [7]. In most of these systems, the large scale properties are described by a zero temperature fixed point, which can be described analytically using the tools of the Functional Renormalization Group (FRG) [8]. This latter has led to very accurate predictions, e.g. concerning various exponents, which could be, in some cases, successfully confronted to experiments or numerical simulations [9].

In some cases, however, thermal fluctuations play an important role: this is the case of systems such that the exponent describing the scale dependence of the fluctuations of the free energy  $\Delta F \sim L^\theta$  is  $\theta = 0$ . It is then crucial to study the interplay between disorder and thermal fluctuations. While at zero temperature Monte-Carlo (MC) simulations, which are hampered by extremely long equilibration times, could be circumvented by the use of powerful algorithms to compute directly the ground states using combinatorial optimization algorithms, the latter are of little use to study finite temperature properties. Here we consider a prototype of such situations, namely the classical 2D XY model with quenched random fields, known as the Cardy-Ostlund (CO) model [13]. It describes a wide class of systems that include 2D periodic disordered elastic systems, such as a randomly pinned planar array of vortex lines [14, 15], surfaces of crystals with quenched disorder [16], random bond dimer models [17] and noninteracting fermions in 2D with disorder [12] (as discussed in [11]). The CO model is defined, in terms of a real phase field  $\theta(\mathbf{x}) \in (-\infty, \infty)$ , by the partition function  $Z = \int \mathcal{D}\theta e^{-H/T}$  where the Hamiltonian  $H$  is given by

$$H = \int d^2x \left[ \frac{\kappa}{2} (\nabla\theta)^2 - \mathbf{f} \cdot \nabla\theta - \frac{1}{a} (\xi e^{i\theta} + \text{h.c.}) \right]. \quad (1)$$

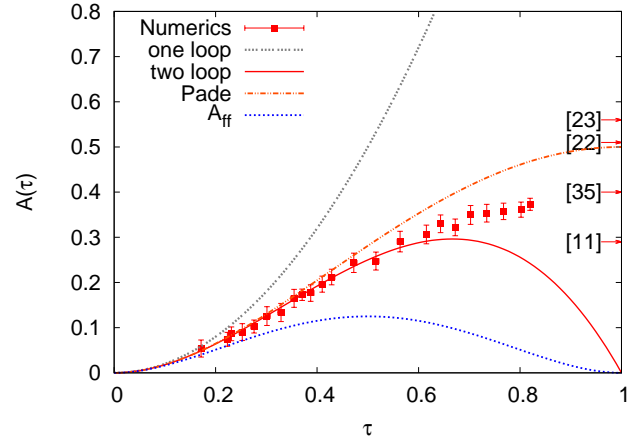


FIG. 1. The amplitude  $A(\tau)$ , characterizing the super-rough phase of the CO model (1), as a function of  $\tau$ . The red points correspond to the numerical estimates obtained here using an exact polynomial algorithm [10]. The curve indexed by 'one loop' indicates the one loop result  $A(\tau) = 2\tau^2$  while the 'two loop' curve shows the two loop result (5) obtained in the present paper [we also show a Padé re-summation of our two loop result (as explained in the text)]. We also show the result  $A_{\text{ff}}$  obtained in [11] from translating to this model the free fermion calculation of Ref. [12]. We have also indicated the values obtained at  $T = 0$  in the corresponding references.

Here  $\kappa$  is the elastic constant,  $a$  is the short-length-scale cutoff, and  $\mathbf{f}$  and  $\xi$  are quenched Gaussian random fields. Their nonzero correlations are given by

$$\overline{f^i(\mathbf{x}) f^j(\mathbf{y})} = T^2 \frac{\sigma}{2\pi} \delta^{ij} \delta(\mathbf{x} - \mathbf{y}), \quad (2)$$

$$\overline{\xi(\mathbf{x}) \xi^*(\mathbf{y})} = T^2 \frac{g}{2\pi} \delta(\mathbf{x} - \mathbf{y}), \quad (3)$$

where  $i, j \in \{1, 2\}$  denotes the components of  $\mathbf{f}$ ,  $T$  is the temperature and  $\overline{\dots}$  denotes the disorder average. The disorder  $\mathbf{f}$  must be introduced in the model as it is generated by the symmetry-breaking field under coarse graining [13]. The CO model exhibits a transition at a critical temperature  $T_c = 4\pi\kappa$  between a high-

temperature phase, where disorder is irrelevant, and a low-temperature glass phase, induced by disorder. This glass phase is described by a line of fixed points indexed by  $T$ , which, thanks to the so-called statistical tilt symmetry (STS), is not renormalized ( $\theta = 0$  to all orders in perturbation theory). It displays many interesting features of glassy systems, e.g. universal sample to sample susceptibility fluctuations [18], and non-equilibrium aging dynamics [19, 20].

The most striking effect of disorder on the static properties concerns the two-point correlation function (CF)  $B(r) = \overline{\langle [\theta(\mathbf{x}) - \theta(\mathbf{x} + \mathbf{r})]^2 \rangle}$ , with  $r = |\mathbf{r}|$ . While for  $T > T_c$  the interface is logarithmically (thermally) rough,  $B(r) \approx 4T/T_c \log(r/a)$ , it becomes superrough for  $T < T_c$  where we have

$$B(r) = A(\tau) \log^2(r/a) + \mathcal{O}(\log(r/a)), \quad (4)$$

where  $\tau = (T_c - T)/T_c$ . The temperature  $T$  is determined by the connected CF  $B_c(r) = \overline{\langle [\theta(\mathbf{x}) - \theta(\mathbf{x} + \mathbf{r})]^2 \rangle_c} \simeq (4T/T_c) \log(r/a)$ . Although the amplitude  $A(\tau)$  of this intriguing  $\ln^2(r)$  has been the subject of numerous studies [18, 21–24], none of them was able to establish a quantitative comparison between analytical results on one hand and numerical simulations on the other, and there are several reasons for this gap. The first one is that  $A(\tau)$  was, analytically, only known, at lowest order in  $\tau$ ,  $A(\tau) = 2\tau^2 + \mathcal{O}(\tau^3)$  [25]: its domain of validity is thus restricted to a narrow region close to  $T_c$ , where the amplitude of the  $\log^2(r)$  term is small and thus extremely hard to isolate accurately from the sub-leading logarithmic correction in (4). The second reason is that numerical simulations are very delicate, given that standard MC simulations are quite inefficient for  $T < T_c$ . Fortunately, there exists an exact polynomial algorithm, called the domino shuffling algorithm (DSA), which allows to sample directly the related random bond dimer model, without running MC simulations. This algorithm was used in Ref. [18], which showed that  $A(\tau) \propto \tau^2$ , without estimating the prefactor. Notice also that, in its original formulation as used in Ref. [18], the DSA suffers from strong finite size effects, which are reminiscent of the arctic circle phenomenon [26] in the pure dimer covering model.

In this Letter, we perform a quantitative comparison, in a wide temperature range, between analytical and numerical predictions. Such a quantitative comparison is rendered possible (i) thanks to a precise calculation of  $A(\tau)$ , using various RG schemes, yielding the following expression to two loop order:

$$A(\tau) = 2\tau^2 - 2\tau^3 + \mathcal{O}(\tau^4), \quad (5)$$

and (ii) thanks to a careful Fourier analysis of the 2-point correlation function. It is computed here using an improvement of the DSA, proposed in Ref. [27], where finite size effects are significantly reduced. The result

of this comparison is shown in Fig. 1 and we see a remarkable agreement between both approaches, even far beyond  $T_c$  down to  $\tau \approx 0.5$ .

Our analytical study is based on the replica method to treat the disorder [28] and obtain the replicated Hamiltonian  $H^{rep} = H_0^{rep} + H_1^{rep}$ , with the harmonic part

$$\begin{aligned} \frac{H_0^{rep}}{T} = & \sum_{\alpha\beta} \int d^2x \left\{ \frac{\kappa}{2T} \delta_{\alpha\beta} [(\nabla\theta_\alpha(\mathbf{x}))^2 + m^2(\theta_\alpha(\mathbf{x}))^2] \right. \\ & \left. - \frac{\sigma}{4\pi} \nabla\theta_\alpha(\mathbf{x}) \cdot \nabla\theta_\beta(\mathbf{x}) \right\}. \end{aligned} \quad (6)$$

The mass  $m$  is introduced in the model as an infrared cutoff and is sent to zero at the end.  $\alpha$  and  $\beta$  denote replica indices and the number of replicas  $n$  is taken to be zero at the end. The system size is infinite. The anharmonic part reads

$$\frac{H_1^{rep}}{T} = -\frac{g}{2\pi a^2} \sum_{\alpha\beta} \int d^2x \cos(\theta_\alpha(\mathbf{x}) - \theta_\beta(\mathbf{x})). \quad (7)$$

Our aim is to compute the two CFs:

$$\mathcal{G}(\mathbf{x}) = \overline{\langle \theta(\mathbf{x})\theta(0) \rangle_H} - \overline{\langle \theta(\mathbf{x}) \rangle_H} \overline{\langle \theta(0) \rangle_H}, \quad (8)$$

$$\mathcal{G}_0(\mathbf{x}) = \overline{\langle \theta(\mathbf{x}) \rangle_H} \overline{\langle \theta(0) \rangle_H}, \quad (9)$$

where the former measures the (disorder averaged) thermal fluctuation while the latter measures the fluctuations due to disorder of the (thermally averaged) phase field. These disorder averaged CFs can be obtained from CFs of replicated fields by decomposing  $\mathcal{G}_{\alpha\beta}(\mathbf{x}) := \overline{\langle \theta_\alpha(\mathbf{x})\theta_\beta(0) \rangle} = \delta_{\alpha\beta}\mathcal{G}(\mathbf{x}) + \mathcal{G}_0(\mathbf{x})$ , where  $\mathcal{G}(\mathbf{x})$  is also called the connected part and  $\mathcal{G}_0(\mathbf{x})$  the off-diagonal part. To compute them we use the harmonic part  $H_0^{rep}$  as the "free" theory and treat  $H_1^{rep}$  in perturbation theory in  $g$ . Here we denote by  $\langle \langle \dots \rangle \rangle$  averages over the complete Hamiltonian  $H^{rep}$  and by  $\langle \dots \rangle$  averages over the free part  $H_0^{rep}$ .

We start by computing the CF for  $g = 0$  and we find

$$G_{\alpha\beta}(\mathbf{q}) = \frac{T}{\kappa} \frac{\delta_{\alpha\beta}}{q^2 + m^2} + \frac{\sigma T^2}{2\pi\kappa^2} \frac{q^2}{(q^2 + m^2)^2} + \mathcal{O}(n). \quad (10)$$

Going to real space one obtains  $G_{\alpha\beta}(\mathbf{x}) = \langle \theta_\alpha(\mathbf{x})\theta_\beta(0) \rangle = \delta_{\alpha\beta}G(\mathbf{x}) + G_0(\mathbf{x})$ . The connected part has the following behavior at small distances  $|x| \ll (cm)^{-1}$

$$G(\mathbf{x}) = -(1 - \tau) \ln [c^2 m^2 (x^2 + a^2)], \quad (11)$$

with the constant  $c = e^{\gamma_E}/2$  and  $\gamma_E$  is the Euler constant. In (11) we have introduced the ultraviolet regularization by the parameter  $a$  [29]. The off-diagonal part of the CF at small distances  $|\mathbf{x}| \ll (cm)^{-1}$  reads  $G_0(\mathbf{x}) = -2\sigma(1 - \tau)^2 \ln [ec^2 m^2 (x^2 + a^2)] + \mathcal{O}(n)$ .

The STS of the model manifests itself by the invariance of the non-linear part  $H_1^{rep}$  under the change  $\theta_\alpha(\mathbf{x}) \rightarrow \theta_\alpha(\mathbf{x}) + \phi(\mathbf{x})$  for an arbitrary function  $\phi(\mathbf{x})$ . As

discussed in Refs. [14, 21, 30] this implies two important properties: (i)  $G_0(\mathbf{x})$  does not appear to any order in perturbation theory in  $g$  in the calculation and (ii) the disorder-averaged thermal CF is uncorrected to all orders  $\mathcal{G}(\mathbf{x}) = G(\mathbf{x})$  i.e. independent of  $g$ . This implies that  $T$  can be *measured* from the amplitude of the logarithm in  $\mathcal{G}(\mathbf{x}) \simeq 2(1 - \tau) \ln x$  at large  $x$ . Because of property (i)  $G_0(\mathbf{x})$  only receives additive corrections, e.g. corrections to  $\sigma$  which, in the present model, change its above logarithmic behavior into a squared-logarithm behavior for  $\mathcal{G}_0(\mathbf{x})$ , obtained below.

In order to obtain the scaling equations beyond lowest order one computes the effective action up to  $\mathcal{O}(g^3)$  terms, which takes the form

$$\Gamma = \sum_{\alpha\beta} \int d^2x \left\{ \frac{\kappa}{2T} \delta_{\alpha\beta} [(\nabla\theta_\alpha)^2 + m^2(\theta_\alpha)^2] - \frac{\sigma_R}{4\pi} \nabla\theta_\alpha \cdot \nabla\theta_\beta - \frac{g_R}{2\pi} c^2 m^2 \cos(\theta_\alpha - \theta_\beta) \right\} \quad (12)$$

in terms of *renormalized* couplings  $g_R$  and  $\sigma_R$ . Their explicit dependence on the bare parameters leads to the following scaling equations in terms of the scale  $\ell = -\ln m$ :

$$\frac{dg_R}{d\ell} = 2\tau g_R - Ag_R^2 - B\tau g_R^2 + Cg_R^3, \quad (13)$$

$$\frac{d\sigma_R}{d\ell} = Dg_R^2 + E\tau g_R^2 - Fg_R^3, \quad (14)$$

and  $d\tau/d\ell = 0$ . Here  $A \dots F$  are *non-universal* constants ( $A, C, D > 0$ ) which satisfy the *universal* ratios

$$A^2/D = 8, \quad A^2/C = 4, \quad F + BD - AE/2 = 0. \quad (15)$$

We have obtained these values through three different regularization schemes, the details are presented in [31]. These equations generalize to two-loop order the one-loop equations obtained in Refs. [13, 14, 16, 21]. The  $\tau$ -equation encodes the exact result  $\mathcal{G}(x) = G(x)$  from STS. From (13) we see that the model has a transition at  $\tau = 0$ , i.e.  $T = T_c$ . For  $T > T_c$  the renormalized coupling  $g_R(\ell)$  flows to zero, while for  $T < T_c$  it flows to a finite value  $g_R^*$  which continuously depends on  $\tau$ :  $g_R^* = 2\tau/A + (4C - 2AB)\tau^2/A^3 + \mathcal{O}(\tau^3)$ . The asymptotic solution of (14) is  $\sigma_R(\ell) \simeq \sigma_0 + [d\sigma(g_R^*)/d\ell]\ell$ : while  $\sigma_0$  depends on all details of the initial condition and leads only to a subdominant single logarithmic growth of the CF, from the second term we obtain the coefficient of the squared logarithmic growth of the CF by a simple argument [16]. To estimate the off-diagonal CF at a given wave-vector  $q$ , one considers the small-mass limit  $m \ll q$  and argues that  $q$  sets the scale  $\ell^* = \ln[1/(aq)]$  at which one stops the RG flow. Replacing  $\sigma$  by its effective value at that scale, i.e.  $\sigma \rightarrow \sigma_R(\ell)$  we get, from (10) the small  $q$  behavior  $\mathcal{G}_0(\mathbf{q}) \simeq 8\pi(1 - \tau)^2 \frac{d\sigma(g_R^*)}{d\ell} \frac{\ln[1/(qa)]}{q^2}$ , which directly leads to (4) and (5). One should notice that the amplitude (5) is *universal* value due to the remarkable combination

of non-universal constants in  $d\sigma(g_R^*)/d\ell$ . Eq. (4) can be obtained more rigorously by calculating the two-point function directly [31].

We have performed simulations to estimate numerically the amplitude  $A(\tau)$  and compare it with our two-loop result (5). For that purpose, we take advantage of the mapping between the CO model and a weighted dimer model defined on a two-dimensional lattice [17, 18], for which there exists a polynomial algorithm, called the "domino shuffling algorithm" [10]. For a technical reason, this algorithm is designed for a special lattice  $A_L$  called the Aztec diamond of size  $L$  (see Fig. 2 for a diamond of size 4). To each bond between nearest neighbors  $(\mathbf{r}, \mathbf{r}')$  on  $A_L$  we assign a quenched random variable  $\epsilon_{\mathbf{r}, \mathbf{r}'}$ : here we consider independent Gaussian random variables, of zero mean and unit variance. The dimer model consists of all complete dimer coverings of  $A_L$ , where the weight  $W(\mathcal{C})$  of a given dimer covering  $\mathcal{C}$  is given by

$$W(\mathcal{C}) = \frac{1}{Z_L} \exp(-H_d/T_d), \quad H_d = \sum_{(\mathbf{r}, \mathbf{r}') \in \mathcal{C}} \epsilon_{\mathbf{r}, \mathbf{r}'}, \quad (16)$$

where  $Z_L \equiv Z_L(\epsilon)$  is the partition function. Hence the limit  $T_d \rightarrow 0$  corresponds to a "strong" disorder regime while the limit  $T_d \rightarrow \infty$  corresponds to dimer coverings with uniform weights. The DSA is based on a recursive procedure which generates a covering of a diamond of size  $L$ ,  $A_L$ , from the covering of a diamond of size  $L - 1$ ,  $A_{L-1}$ . It generates uncorrelated dimer configurations, directly sampled with the equilibrium weight (16), without the need to run a slow MC algorithm. In addition, this is a polynomial algorithm (with a computational time growing like  $L^3$ ). The dimer covering of the Aztec diamond is however known to suffer from very strong finite size effects, known under the name of the arctic circle phenomenon [26]. Here we minimize significantly these effects by using a recent improvement of the DSA which allows for the existence of bonds with zero weight [27]. We use it to study the random dimer model directly on a square lattice, which exhibits less pronounced finite-size effects [32].

From a given dimer covering  $\mathcal{C}$ , it is possible to assign a discrete two-dimensional height field, defined on the center of the squares (see Fig. 2), i.e. on the dual  $A_L^D$  of  $A_L$ , as follows [33]. The bonds of  $A_L^D$  are oriented such that the unit cells of  $A_L^D$  that enclose the blue sites of  $A_L$  (see Fig. 2) are circled counterclockwise. Assign  $-3$  to the difference of neighboring heights along the oriented bonds if a dimer is crossed and  $+1$  otherwise. This yields single-valued heights up to an overall constant, the heights on the boundaries of  $A_L$  being then fixed as in Fig. 2. This defines a height field  $\tilde{H}_{\mathbf{r}} \equiv \tilde{H}_{ij}$ , with  $\mathbf{r} = i\mathbf{u}_x + j\mathbf{u}_y$  and the relative height  $h = \tilde{H} - \langle \tilde{H} \rangle$  where  $\langle \tilde{H} \rangle$  is a spatial average of  $\tilde{H}$  over the whole diamond. For uniform dimer coverings, corresponding to  $\epsilon_{\mathbf{r}, \mathbf{r}'} = 0$  or  $T_d \rightarrow \infty$ , one can show that the fluctuations of  $h$  in the continuum

limit (and in the bulk of the diamond, see below) are described by a Gaussian free field [33, 34], *i. e.* by the Hamiltonian in Eq. (1) without disorder ( $\mathbf{f} = 0$ ,  $\xi = 0$ ) at  $\tau = 1 - T/T_c = 0$ . In the presence of inhomogeneous random bond variables  $\epsilon_{\mathbf{r},\mathbf{r}'}$  one expects instead that in the continuum limit (and in the bulk of the diamond, see below), the fluctuations of  $h$  are described by the CO model (1) with the substitution  $\theta \rightarrow h \times 2\pi/4$  [17, 18]. This factor  $2\pi/4$  is required because one can check that the energy associated to the height configurations (16) is invariant under a global shift  $h \rightarrow h + 4$ .

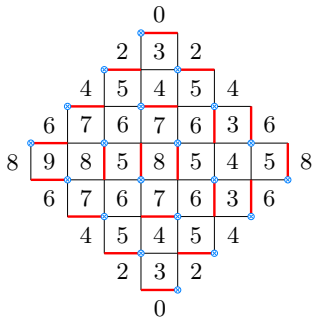


FIG. 2. Dimer covering of an Aztec diamond of size 4,  $A_4$ . On each bond there is a random variable  $\epsilon_{\mathbf{r},\mathbf{r}'}$  which determines the weights assigned to each dimer covering (16). As explained in the text, the blue points are useful to define the height field, which are the integer numbers in the squares and form the dual lattice  $A_4^D$ .

The temperature  $T_d$  of the dimer model does not coincide with the temperature of the CO model in Eq. (1). To compute the dimensionless temperature  $\tau = 1 - T/T_c$ , we use the STS which allows to measure this parameter from the connected CF (8). Indeed we compute

$$W_T^2 = \frac{1}{L^2} \sum_{\mathbf{r}} \overline{\langle h_{\mathbf{r}}^2 \rangle - \langle h_{\mathbf{r}} \rangle \langle h_{\mathbf{r}} \rangle} \simeq 2(1 - \tau) \log L, \quad (17)$$

which provides a precise estimate of the parameter  $\tau$ . We have also checked that our numerical estimate is in good agreement with the analytic results, not only for this parameter but also for other thermodynamical observables like the entropy or the internal energy, obtained in Ref. [17].

We want to compute numerically the amplitude of the  $\log^2(r)$  term in Eq. (4). Extracting this amplitude precisely from the two-point correlation function is however difficult, since the subleading corrections are of order  $\mathcal{O}(\log r)$ . The calculation is more accurate in Fourier space [22, 35], defining  $\hat{h}_{\mathbf{q}} = L^{-2} \sum_{\mathbf{r}} h_{\mathbf{r}} e^{i\mathbf{q}\cdot\mathbf{r}}$ . The CF  $C(q)$  of these Fourier components is expected, from Eq. (4), to behave for small  $q$  as

$$C(q) = \overline{\langle \hat{h}_{\mathbf{q}} \rangle \langle \hat{h}_{-\mathbf{q}} \rangle} \simeq \frac{8}{\pi} A(\tau) \frac{\log(1/q)}{q^2} + \mathcal{O}(q^2), \quad (18)$$

where  $q = |\mathbf{q}|$ . In Fig. 3, we show a plot of  $q^2 C(q)$  as a function of  $q$  in linear-logarithmic scales for  $\tau \approx 0.33$  ( $T_d = 0.25$ ). These data have been obtained for a system size  $L = 384$  and by averaging over  $10^5$  independent realizations of the random bonds  $\epsilon_{\mathbf{r},\mathbf{r}'}$ 's. These data

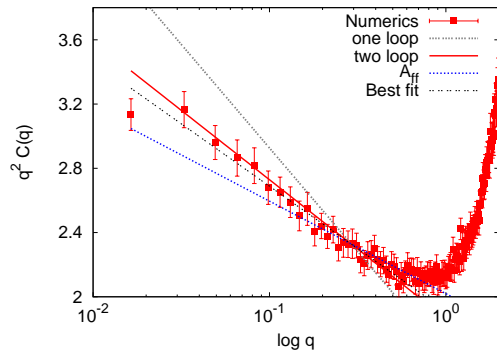


FIG. 3. Plot of  $q^2 C(q)$  as a function of  $\log q$ . The red symbols correspond to our numerical data obtained for a lattice of size  $L = 384$ . The slope of the straight line indexed by 'one loop' and 'two loop' is given respectively by the one loop  $A(\tau) = 2\tau^2$  and the two loop estimate in Eq. (5), while the slope of the straight line indexed by  $A_{\text{ff}}$  is the one corresponding to Ref. [12].

support the expected behavior in Eq. (18) for small  $q$ ,  $q \lesssim 1$ : they are indeed well described by a straight line,  $q^2 C(q) = -8A(\tau)/\pi \log q + b_0$ . Note that the downwards bending of the numerical data observed in Fig. 3 for the smallest  $q$ 's is a finite size effect. In this figure we also show four different straight lines corresponding to four such different couples  $(A(\tau), b_0)$ . The line indexed by 'Best fit' corresponds to the best fit of these data by a straight line: the value of  $A(\tau)$  obtained in this way allows us to compute  $A(\tau)$  for different values of  $\tau$ , as shown on Fig. 1. In the three other cases, the slope of this straight line is evaluated from the one-loop and two-loop (5) results respectively, while the straight line indexed by ' $A_{\text{ff}}$ ' corresponds to the slope computed in [11] from the result in Ref. [12], with  $A_{\text{ff}}(\tau) = 2\tau^2(1 - \tau)^2$ . In all cases the constant  $b_0$  is a fitting parameter. One clearly sees that the two loop result is a significant improvement over the one loop result and describes very well our numerical data. In addition, we also see that  $A_{\text{ff}}$  clearly underestimates our numerical data.

Let us now discuss the numerical results for  $A(\tau)$  plotted as a function of  $\tau$  in Fig. 1. As compared to Ref. [18], here we can discuss a much broader range of values of  $\tau$  which extends deep into the glass phase. First we observe that our two loop result is in very good agreement with our numerics up to  $\tau \approx 0.5$ . In contrast, the curve  $A_{\text{ff}}(\tau)$  is significantly smaller than our numerical values and can be ruled out. For smaller temperature,  $\tau \gtrsim 0.5$  the discrepancy between our two loop result and the numerical value increases, as expected. In Fig. 1 we have also

quoted the numerical values which were obtained independently at zero temperature by an exact ground state calculation for the SOS model on a disordered substrate in Refs. [22, 23, 35]. This model is also believed to be described, in the continuum limit, by the CO model (1). In particular, our data match smoothly with the most recent, and probably the most accurate, numerical estimate obtained in Ref. [35], yielding  $A(\tau = 0) = 0.39$ . We also show an estimate based on a one-loop FRG calculation at  $T = 0$  [11]. The fact that the two loop formula (5) vanishes at  $T = 0$  is of course an unphysical feature, which can be cured by considering various guesses or Padé (i.e. rational functions in  $\tau$ ) approximations which have the same expansion as (5) to order  $\tau^3$ . One such formula  $A(\tau) = 2\tau^2(1 - \tau/2)^2$  is plotted in Fig. 1: in addition to being simple it has a reasonable structure to correct the result of Ref. [12].

In conclusion, we have obtained an accurate description of the low temperature glass phase of the Cardy-Ostlund model (without vortices) down to temperatures  $T_c/2 \lesssim T$ , with excellent agreement for the amplitude of the square logarithm between theory and numerics. Understanding the glass phase below  $T_c/2$  is an important challenge for the future.

This research was supported by ANR grant 09-BLAN-0097-01/2 and by ANR grant 2011-BS04-013-01 WALK-MAT.

- 
- [1] S. Lemerle, J. Ferre, C. Chappert, V. Mathet, T. Giamarchi, and P. Le Doussal, Phys. Rev. Lett. **80**, 849 (1998)
- [2] P. Paruch, T. Giamarchi, and J.-M. Triscone, Phys. Rev. Lett. **94**, 197601 (2005)
- [3] S. Moulinet, C. Guthmann, and E. Rolley, Eur. Phys. J. E **8**, 437 (2002)
- [4] S. Santucci, K. J. Maloy, A. Delaplace, J. Mathiesen, J. O. H. B. A. Hansen, J. Schmittbuhl, L. Vanel, and P. Ray, Phys. Rev. E **75**, 016104 (2007)
- [5] G. Blatter, M. V. Feigelman, V. B. Geshkenbein, A. I. Larkin, and V. M. Vinokur, Rev. Mod. Phys. **66**, 1125 (1994)
- [6] T. Giamarchi, arXiv:cond-mat/0403531(2004)
- [7] G. Gruner, Rev. Mod. Phys. **60**, 1129 (1988)
- [8] P. Le Doussal, Ann. Phys. **325**, 49 (2010)
- [9] K. J. Wiese and P. Le Doussal, Markov Proc. Relat. Fields **13**, 777 (2007)
- [10] J. Propp, Theor. Comp. Sci. **303**, 267 (2003)
- [11] P. Le Doussal and G. Schehr, Phys. Rev. B **75**, 184401 (2007)
- [12] S. Guruswamy, A. LeClair, and A. W. W. Ludwig, Nucl. Phys. B **583**, 475 (2000)
- [13] J. L. Cardy and S. Ostlund, Phys. Rev. B **25**, 6899 (1982)
- [14] T. Hwa and D. S. Fisher, Phys. Rev. Lett. **72**, 2466 (1994)
- [15] C. A. Bolle, V. Aksyuk, F. Pardo, P. L. Gammel, E. Zeldov, E. Bucher, R. Boie, D. J. Bishop, and D. R. Nelson, Nature **399**, 43 (1999)
- [16] J. Toner and D. P. DiVincenzo, Phys. Rev. B **41**, 632 (1990)
- [17] S. Bogner, T. Emig, A. Taha, and C. Zeng, Phys. Rev. B **69**, 104420 (2004)
- [18] C. Zeng, P. L. Leath, and T. Hwa, Phys. Rev. Lett. **83**, 4860 (1999)
- [19] G. Schehr and P. Le Doussal, Phys. Rev. Lett. **93**, 217201 (2004)
- [20] G. Schehr and H. Rieger, Phys. Rev. B **71**, 184202 (2005)
- [21] D. Carpentier and P. Le Doussal, Phys. Rev. B **55**, 12128 (1997)
- [22] C. Zeng, A. A. Middleton, and Y. Shapir, Phys. Rev. Lett. **77**, 3204 (1996)
- [23] H. Rieger and U. Blasum, Phys. Rev. B **55**, R7394 (1997)
- [24] D. J. Lancaster and J. J. Ruiz-Lorenzo, J. Stat. Mech., P01003(2007)
- [25] Note that various values of the  $\tau^2$  coefficient have appeared in the literature before it was fixed in Ref. 21
- [26] P. S. W. Jockush, J. Propp, Preprint available at arxiv.org/abs/math.CO/9801068(1998)
- [27] E. Janvresse, T. de la Rue, and Y. Velenik, Electron. J. Combin. **13(1)**, R30 (2006)
- [28] T. Giamarchi, *Quantum Physics in One Dimension* (Clarendon press, Oxford, 2003)
- [29] D. J. Amit, Y. Y. Goldschmidt, and G. Grinstein, J. Phys. A **13**, 585 (1980)
- [30] U. Schulz, J. Villain, E. Brézin, and H. Orland, J. Stat. Phys **51**, 1 (1988)
- [31] Z. Ristivojevic, P. Le Doussal, and K. Wiese, (in preparation)(2012)
- [32] A. Perret and G. Schehr, (in preparation)
- [33] C. L. Henley, J. Stat. Phys. **89**, 483 (1997)
- [34] R. Kenyon, Ann. Probab. **28**, 1128 (2001)
- [35] K. Schwarz, A. Karrenbauer, G. Schehr, and H. Rieger, J. Stat. Mech., P08022(2009)